25th IAHR International Symposium on Ice

Trondheim, June 14 to 18, 2020

Ice Formation in Norwegian Fjords – Findings from the 2018 - 2019 Field Season

M. O'Sadnick[1,2], C. Petrich[1], Ø. Kleven[1], J. Skarðhamar[3] & C. Brekke[2]

[1]SINTEF Narvik, Narvik, Norway

[2]UiT The Arctic University of Norway, Tromsø, Norway

[3] Institute of Marine Research, Tromsø, Norway

megan.osadnick@sintef.no, christian.petrich@sintef.no, oystein.kleven@sintef.no, jofrid.skardhamar@imr.no, camilla.brekke@uit.no

Understanding ice conditions in fjords is imperative to ensure safe operations and to protect the surrounding environment. Seven fjords in northern Norway were visited in March 2019, six with significant ice cover. In each location, measurements of ocean temperature and salinity, and $\delta^{18}O$ for ocean water and river water leading into the fjords were gathered. In addition, where ice was present, measurements of ice bulk salinity and $\delta^{18}O$ were obtained along with an extra core to examine ice stratigraphy and pore structure. Results show ice of low bulk salinity, < 1.5 psu, and $\delta^{18}O$, < -7.67 ‰, in five fjords holding ice with maximum ice thickness being upwards of 0.46 m. This result combined with examination of stratigraphy cores reveals ice closely resembling freshwater ice in structure despite lying atop an ocean of average salinity 32 – 33.5 (psu). Ice salinity profiles elude to varying environmental conditions impacting ice formation throughout the winter season. Due to the impact of significant freshwater flux, ice properties differed significantly from sea ice forming in the open ocean, an important characteristic when considered in application to coastal operations.

1. Introduction

The coast of mainland Norway is dominated by the presence of fjords cutting into the adjacent mountains, with the glaciers that carved these fjords receded into higher terrain if not gone entirely (Holtedahl, 1967; Porter, 1989). Often subjected to temperatures below freezing, ice has the possibility to form in Norwegian fjords. While the Norwegian pilot guide offers brief descriptions of ice conditions in selected areas to assist boat and ship captains (Hughes, 2006), no studies exist that make direct observations of sea ice thickness, extent and properties in fjords found throughout mainland Norway. Ice conditions in the pilot guide are themselves based primarily off aging data published in older editions mixed with examination of visible and infrared satellite images gathered in February and March 2005.

The fjords in mainland Norway are influenced by the North Atlantic current bringing warm waters into the fjords, which therefore are mainly ice free all year. However, smaller side fjords and the inner parts of larger fjords often freeze up during winter, a subject of little focus in scientific research until now (O'Sadnick et al 2018; 2020). There is a wide breadth of published work from mainland Norwegian fjords during ice free conditions (for example Asplin et al., 1999; Eilertsen & Skardhamar, 2006; Lalande et al., 2020; Mankettikkara, 2013; Myksvoll, 2008; Myksvoll et al., 2013; Skardhamar et al., 2018). These studies examine the fjord system from physical and biological perspectives, both of which are potentially impacted by the presence of ice. When ice forms on the surface of a fjord, it creates a barrier between the ocean and air, altering the exchange of mass and energy (Petrich & Eicken, 2010) . In addition, ice creates a biologically rich environment of brine-filled pores that offers a sheltered place for algae and other microbiota to grow (Arrigo et al, 2010; Brandon et al., 2010). These processes are well understood in studies of sea ice in the open ocean. In addition, studies of sea ice in the Baltic Sea offer descriptions of ice grown from sea water of lower salinity, brackish in character, as well as the impact of fresh water plumes on local ecology (Granskog et al. 2005a; Granskog et al., 2005b; Kaartokallio et al., 2007). While such knowledge can be applied to fjord ice, adaptations must be made to account for a stratified water column with saline sea water overlain by a layer of very low or even fresh water, different from the brackish water of the Baltic. Given increasing interest in Norway from both shipping and resource exploration industries, the safety hazard and potential obstacle ice presents to operations are of concern. Therefore, understanding ice conditions and how they vary from fjord to fjord, throughout the year, and between years as the climate changes is important from both a scientific and operational perspective.

2. Methods

2.1. Ice sampling

Seven fjords were chosen based on previous observations of ice formation in recent years. For the 2018 – 2019 season, all but one fjord, Storfjord, held ice. Ice sampling location was chosen based on accessibility and total extent of the ice. The locations of sampling sites are shown in Fig. 1. Typically, samples were gathered in approximately the center of the fjord, 1 – 2 km from the head of the fjord where a river input was present. Snow depth was first measured and samples collected for $\delta^{18}O$ measurements before a section was cleared of snow. A Kovacs ice core barrel, 10 cm in diameter, was used with a hand drill to collect at least two ice cores at each location – one for bulk salinity and the other for stratigraphy analysis. For the former, ice was sliced into 5 cm sections and bagged for melting on return to the lab. Sample salinity was measured using a YSI Pro-30 salinometer with an accuracy of 0.1 on the practical salinity scale (psu) and

resolution of ±0.1 (psu) or ±1% of the reading, whichever is greater. Once melted samples were measured, they were poured into glass viles and closed with a cone lined cap before being stored at 5 °C until $\delta^{18}O$ could be measured. Samples were analyzed at the Stable Isotope Laboratory at the Centre for Arctic Gas Hydrate, Environment and Climate (CAGE) located at UiT – The Arctic University of Norway, Tromsø, Norway. A 0.3 mL sample from each melted core slice was pipetted into a 12 mL Labco glass vial which was next flushed with a 0.3% CO2 in He gas mixture, equilibrated at 25°C for <24h. Calibration was done through measuring three inhouse standards of $\delta^{18}O$ between -1 ‰ and -36 ‰ that had previously been calibrated against international standards VSMOW2, GISP, and SLAP2. When a line was fit to true vs. measured vales of $\delta^{18}O$, the R^2 value of the line was 1.0, with error between separate readings most often being less than 0.01 ‰ but with a standard deviation <0.05 ‰. A Thermo-Fisher MAT253 IRMS with a Gasbench II was used to measure the quantity of $\delta^{18}O$ defined as

$$\delta^{18}O = \left(\frac{\left(\frac{^{18}O}{^{16}O}\right)_{sample}}{\left(\frac{^{18}O}{^{16}O}\right)_{standard}} - 1 \right) * 1000 \quad (1)$$

where the standard is Vienna Standard Mean Ocean Water (VSMOS).

Brine volume fraction was calculated using measured values of bulk salinity and a modelled linear temperature profile that assumed an air/ice temperature of -2 °C and an ice/ocean temperature of 0 °C (Leppäranta & Manninen, 1988).

Stratigraphy samples were kept in a cooler during transport to their storage location. They were stored at -30 °C and processed in a cold room at -15 °C. They were sliced to a thickness of 12 – 16 mm and examined on a light table for pore structure and layering. Additionally, cross polarized filters were used to clarify crystal structure and further highlight transitions in the ice.

2.2. Water sampling

In addition to melted ice samples, seawater and river water was also gathered for measurement of $\delta^{18}O$. For seawater measurements, a tube, 1 cm in diameter, was lowered to the pre-determined depth with the end above water plugged. The plug was then released, allowing water from that depth to fill the tube, before being plugged again and raised to the surface to fill the same cone lined bottles described above. Each bottle was first rinsed with water from the same depth before being filled. In addition to seawater, water samples from rivers leading into each fjord were gathered.

2.3. Satellite and photo image processing

UOVision UM 565 and UM785 trail cameras were used to collect timelapse images of several fjords. Examples of the photos obtained are presented in Fig. 2. Additionally, images from the SENTINEL-1 C-band Synthetic aperture radar (SAR), vertical transmit/vertical received (VV) were examined to determine when ice formed, termed a freeze-up date here, to within 2 – 3 days for fjords having no camera (Copernicus, 2019). Due to the difficulty of identification, visual inspection of individual images was needed to confirm the presence of ice.

Imagery from the Terra satellite MODIS sensor, specifically MOD09A1.006 Terra Surface Reflectance 8-Day Global 500m was also used to track ice from February, when sunlight has returned to northern Norway, through May to determine a date when fjords were ice free to

within 8 days (Vermote, 2015). MODIS Images were first processed to exclude any pixels of low quality or marked as having clouds. Next, the following formula was applied:

$$Ice\ band = Band\ 3\ [459 - 479\ nm] - (Band\ 6\ [1628 - 1652\ nm] + Band\ 7\ [2105 - 2155\ nm]) \quad (2)$$

Pixels having above a certain value were then classified as ice. This method is similar to that used in Petrich et al. (2017) but automated to allow for a larger number of images to be processed. Processing steps are described in more depth in O'Sadnick et al. (2020).

3. Results & Discussion

3.1. Linking source water to ice

A summary of the dates of ice formation and breakup are presented in Table 1. Ice was observed in Sørbotn/Ramfjord for the longest period of time, 20 December 2018 to 7 May 2019. Kattfjord was second with ice being present from 14 January to 26/27 April 2019. In the remaining fjords, the ice season was shorter: 27 – 29 January to 16 - 24 April 2019 in Gratangen, 3 March to 21 April 2019 in Beisfjord, 20 – 23 January to 16 - 24 April 2019 in Lavangen, and 29 – 30 January to 16 - 24 April 2019 in Nordkjosbotn. Additionally, Storfjord was shown to hold small amounts of ice through the season but only near the outlet river and over short stretches of time. This is supported by timelapse and MODIS images (not shown). The conditions that enable ice formation in fjords are difficult to define due to the changing balance between ocean salinity and temperature (conditions influenced by weather, tides, and currents), freshwater flux into the fjord, the resultant stratification, and air temperature. To fully understand the evolution of fjord ice from beginning to end, further observation and study is needed to determine the dominant factors and how these may change between fjords and with time.

Measurements of water temperature and salinity gathered in each fjord are shown in Fig.3. Gratangsbotn was warmest with water temperatures above 6 °C at depth while Nordkjosbotn was coldest, dipping below 1 °C The other four fjords had temperatures generally between 3 – 4 °C. All had a fairly constant salinity between 32 and 33.5 psu with the most variation seen in the upper 2 m. Note, the upper 1 m of each profile is not shown as it may have been disturbed by the coring. At five fjords, a single location was selected to collect measurements and acquire ice cores for further processing. At one fjord, Beisfjord, several locations were visited (Fig. 1). Thick sections, measurements of salinity and $\delta^{18}O$, and calculated brine volume fraction for Sørbotn/Ramfjord, Kattfjord, and four location in Beisfjord, are presented in Figs. 4 – 9 respectively. Additionally, bulk salinity and brine volume fraction are provided in Fig.10 for Gratangsbotn, Lavangen, and Nordkjosbotn.

In six out of the seven cores gathered, salinity did not increase above 1.2 psu with Sørbotn/Ramfjord, Kattfjord, and Gratangsbotn having bulk salinity consistently below 0.5 psu. In all other cores where $\delta^{18}O$ was measured, values ranged from -7.73 ‰ (Kattfjord) down to -12.17 ‰ (Beisfjord 1). In cores from Ramfjord, Beisfjord 3, and Beisfjord 4, bulk salinity and $\delta^{18}O$ largely parallel each other having similar increases and decreases through their entire depth. In cores from Kattfjord, Beisfjord 1, and Beisfjord 2, these two measurements sometimes mimic each other but also show instances of being opposite- in the core gathered from Kattfjord for example, an increase in bulk salinity at a depth of 20-25 cm from 0.2 to 0.3 psu, coincides with a decrease in $\delta^{18}O$ from -7.67 to -8.76 ‰. The relationship between bulk salinity and $\delta^{18}O$ is non-

trivial being dependent on the source of water as well as the ice growth rate. Seawater has a $\delta^{18}O$ value between – 1 to 0 ‰ while fresh water, from river runoff specifically, ranged here from -10.24 to -12.49. Values of $\delta^{18}O$ in the upper 1 m of ocean water from each sampling site as well as river water entering the fjord are summarized in Table 2. While a decrease in salinity is often linked to a decrease in $\delta^{18}O$, in fjord ice this is not always the case. As growth rate of ice slows, the ratio of ^{18}O to ^{16}O increases due to ^{18}O being incorporated preferentially, the reason related to differences in molecular vibration energy (Eicken, 1998). Resultantly, $\delta^{18}O$ will be greater (less negative, or at times positive) in ice formed at a slower versus a faster rate. Bulk salinity is also affected by growth rate with slower growth leading to lower salinity, faster growth to higher salinity (Petrich et al., 2011). Therefore, ice formed from water of comparatively higher salinity but grown quickly may have a comparable $\delta^{18}O$ value for ice formed from water of lower salinity but at a slow growth rate. In such a case however, values for bulk salinity would further diverge.

In only one core were values of salinity higher than 2 psu and $\delta^{18}O$ higher than -7 ‰ measured, that being Beisfjord 4 (Fig. 9). Bulk salinity decreased from 5.6 psu in the upper 3 cm to 0.6 psu at the ice/ocean interface, a depth of 18 cm. Similarly, this core also had the highest value of $\delta^{18}O$, -2.58 ‰ in the upper 3 cm, decreasing to -9.41 ‰ at its bottom. The highest values for bulk salinity and $\delta^{18}O$ occur in granular ice formed likely through the flooding of the snow-covered surface. The core was collected at the edge of a transition -- nearer to the head of the fjord and entrance of the river, ice was consistently > 20 cm, on the other side of the transition, ice was < 10 cm (Beisfjord 3 core, Fig.8). Beisfjord 3 presumably formed at a later time given its thickness of only 8 cm. Comparing the two cores, a change in microstructure and crystal structure approximately 10 cm in the Beisfjord 4 core, aligns with the top of the Beisfjord 3 core in salinity and $\delta^{18}O$. Additionally, a layer of transparent, glass-like ice was found at the bottoms of both cores. This indicates consistency in the water that formed the lower section of Beisfjord 4 sample and the entirety of the Beisfjord 3 sample. The weather leading up to the field visit was consistently cold, with a daily average air temperature consistently below -4 °C. While this would indicate likely no large increase in fresh water, snowfall was recorded twice in the short period of time from ice formation to the field visit (not shown). This snowfall may have led to an increase in flux from the river or alternatively, a layer of freshwater to form on the surface of the fjord that enabled the formation of the Beisfjord 3 core and which later flowed under the ice as the tide rose.

Each core has a mixture of granular (frazil) and congelation ice with all also displaying several changes in microstructure. For example, in the upper 10 cm of the Beisfjord 1 core, texturally classified as granular, pores are spherical and large in comparison to the next 5 cm of granular ice where pores decrease significantly is size and increase in density. At a depth of 15 cm, where a transition to congelation ice occurs, the number of pores decreases with their shape also changing to be generally thin and elongated. Layers exist within this microstructure however where there are several pores clearly larger in size, lengthening in steps downwards, from approximately 0.5 cm, to 1.0 cm, 1.5 cm, and finally 2.5 cm in the lower 10 cm of the core. Salinity relatedly decreased slightly from 0.3 to 0.2 psu while $\delta^{18}O$ increased from -10.50 to -10.06 ‰. This provides one example where salinity and $\delta^{18}O$ not aligning may be due to growth rate. We hypothesize that the water at the interface remained constant in its $\delta^{18}O$ and salinity values as ice grew while ice growth slowed due to the thickening of ice, the accumulation of snow on the surface, changes in air and ocean temperature, or a mix of these factors.

In cores gathered in Ramfjord and Kattfjord, several transitions in microstructure and relatedly bulk salinity and $\delta^{18}O$ are evident. It is difficult to define with certainty the cause of each change. However, examining weather data from these two fjords both experienced snowfall and rainfall/snowmelt that may have altered properties of the water at the ice/ocean interface. Additionally, abrupt changes in pore size like that found at 25 cm in the Kattfjord core bring to light other factors that may disrupt conditions at the ice/ocean interface. While the ice protects much of the underlying ocean from turbulence, wind and tides/currents still have potential to disrupt conditions at the ice/water interface that may lead to variations in ice microstructure. To better understand how these layers of differing microstructure, salinity, and $\delta^{18}O$ develop, continuous observation of environmental conditions is needed.

3.2. Implications

As marine traffic increases, the risk of an oil spill, either from ships or oil production, is becoming more of a concern. Oil emplaced under and frozen into sea ice having a well-understood microstructure of connected brine pores and channels would have a pathway to rise to the surface during spring warming as pores connect (Dickens, 2011; Petrich et al., 2013). If layers of lower porosity or possibly impermeable, freshwater, ice are present, this process will be disrupted resulting in a different oil clean up scenario. In Figs 4 - 9, brine volume fraction was investigated to examine how ice may evolve in warm temperatures when one would expect the pore space to become more connected. In a previous studies by Karlsson et al. (2011), it was estimated that oil migration occurred around 10% brine volume fraction but often not until ice reached even greater values of upwards 15 % brine volume fraction. In five out of the six cores collected, brine volume fraction does not exceed 6 %. It is only the Beisfjord 4 sample, where portions of the ice are above the 10 % threshold with no ice above 15 %. Parts of the core do remain below 10 % however meaning that while oil would possibly be able to migrate upwards it would likely hit a barrier slowing or preventing oil movement to the surface.

Transitions in sea ice microstructure from congelation, columnar ice to granular, frazil ice have also been shown to disrupt and alter how oil rises to the surface even when values for brine volume fraction are high (Oggier et al., 2019). The cores presented here all had transitions as well as several layers of clearly differing pore size and density which could potentially impact the behavior of oil in the ice. Hence, for the cores included in this study, timing of oil surfacing for potential clean up would be likely be difficult to predict.

4. Conclusions

Seven fjords were visited in the northern Norway in March of 2019 with six having ice of thickness ranging from 8 – 46 cm, that was subsequently cored and sampled. Seawater ranged in salinity from 32 to 33.5 psu underneath the ice while bulk ice salinity stayed below 1.5 psu for five out of six fjords, increasing up to 5.8 psu in the remaining core. Measurements of $\delta^{18}O$ largely stayed below -7.67 ‰. The sixth core with high salinity, remained an outlier however having $\delta^{18}O$ values reaching as high as -2.58 ‰.

When examining thick sections, pores of varying shape and size were apparent with many cores holding a mixture of spherical pores of differing diameter and density, thin elongated pores interspersed in relatively transparent ice, occasional brine channels several centimeters in length, and also sections of ice devoid of any pores. The date of ice formation was determined through timelapse images and estimations from ice thickness and air temperature. It is hypothesized here

that changing weather conditions resulting in fluctuations in air temperature, snowfall, and runoff from rainfall/snowmelt contributed to layers of differing pore structure. Continuous observations are needed to observe ice formation as well as changes in river input to further support this point. In addition, a greater number of $\delta^{18}O$ measurements taken consistently at the same locations and throughout the year, will further clarify how river water influences ice formation throughout the winter season.

Acknowledgements

This work was funded by the Centre for Integrated Remote Sensing and Forecasting for Arctic Operations (CIRFA), a Centre for Research- based Innovation (Research Council of Norway project number 237906).

References

Anderson, D. L. (1961). Growth rate of sea ice. *Journal of Glaciology*, *3*(30), 1170–1172.

Arrigo, K. ., Mock, T., & Lizotte, M. . (2010). Primary Producers and Sea Ice. In D. . Thomas & G. . Dieckmann (Eds.), *Sea Ice* (1st ed., pp. 283–326). Oxford: Wiley-Blackwell.

Asplin, L., Salvanes, A. G. V., & Kristoffersen, J. B. (1999). Nonlocal wind-driven fjord-coast advection and its potential effect on plankton and fish recruitment. *Fisheries Oceanography*, *8*(4), 255–263. https://doi.org/10.1046/j.1365-2419.1999.00109.x

Brandon, M. ., Cottier, F. ., & Nilsen, F. (2010). Sea Ice and Oceanography. In D. N. Thomas & G. Dieckmann (Eds.), *Sea Ice* (1st ed., pp. 79–112). Oxford: Wiley-Blackwell.

Copernicus Sentinel data (2019) for Sentinel data, processed by ESA.

Dickens, D. (2011). Behavior of oil spills in ice and implications for Arctic spill response. In *OTC Arctic Technology Conference*. Offshore Technology Conference.

Eicken, H. (1998). Deriving Modes and Rates of Ice Growth in the Weddell Sea from Microstructural, Salinity and Stable-Isotope Data. *Antarctic Sea Ice: Physical Processes, Interactions and Variability, Antarct. Res. Ser*, *74*, 89–122. https://doi.org/10.1029/ar074p0089

Eilertsen, H. C., & Skardhamar, J. (2006). Temperatures of north Norwegian fjords and coastal waters: Variability, significance of local processes and air-sea heat exchange. *Estuarine, Coastal and Shelf Science*, *67*(3), 530–538. https://doi.org/10.1016/j.ecss.2005.12.006

Granskog, M. A., Ehn, J., & Niemelä, M. (2005). Characteristics and potential impacts of under-ice river plumes in the seasonally ice-covered Bothnian Bay (Baltic Sea). *Journal of Marine Systems*, *53*(1–4), 187–196. https://doi.org/10.1016/j.jmarsys.2004.06.005

Granskog, M. A., Kaartokallio, H., Thomas, D. N., & Kuosa, H. (2005). Influence of freshwater inflow on the inorganic nutrient and dissolved organic matter within coastal sea ice and underlying waters in the Gulf of Finland (Baltic Sea), *65*, 109–122. https://doi.org/10.1016/j.ecss.2005.05.011

Holtedahl, H. (1967). Notes on the Formation of Fjords and Fjord-Valleys. *Geografiska Annaler.*

Series A, Physical Geography, *49*(2), 188–203.

Hughes, N. (2006). *NP57A, NP57B, NP58A, NP58B Norway Pilot. Sea Ice Conditions: West coast of Norway from: Lindesnes to Statlandet, Statllandet to Risværfjorden. Offshore and coastal waters of Norway from: Risværfjorden to the north part of Vesterrålen, Andfjorden to Varang*. Argyll, UK: Scottish Association for Marine Science.

Kaartokallio, H., Kuosa, H., Thomas, D. N., Granskog, M. A., & Kivi, K. (2007). Biomass , composition and activity of organism assemblages along a salinity gradient in sea ice subjected to river discharge in the Baltic Sea. *Polar Biology*, *30*, 183–197. https://doi.org/10.1007/s00300-006-0172-z

Karlsson, J., Petrich, C., & Eicken, H. (2011). Poac'11, (Amsa 2009).

Lalande, C., Dunlop, K., Renaud, P. E., Nadaï, G., & Sweetman, A. K. (2020). Seasonal variations in downward particle fluxes in Norwegian fjords. *Estuarine, Coastal and Shelf Science*, *241*. https://doi.org/10.1016/j.ecss.2020.106811

Leppäranta, M., & Manninen, T. (1988). *The brine and gas content of sea ice with attention to low salinities and high temperatures*. Helsinki.

Mankettikkara, R. (University of T. (2013). Hydrophysical characteristics of the northern Norwegian coast and fjords. *Dissertation for the Degree of Philosophiae Doctor*, (August).

Myksvoll, M. S. (2008). *Mechanisms affecting the transport of early stages of Norwegian coastal cod - a fjord study*. The University of Bergen.

Myksvoll, M. S., Erikstad, K. E., Barrett, R. T., Sandvik, H., & Vikebø, F. (2013). Climate-driven ichthyoplankton drift model predicts growth of top predator young. *PLoS ONE*, *8*(11). https://doi.org/10.1371/journal.pone.0079225

O'Sadnick, M., Petrich, C., Brekke, C., & Skarðhamar, J. (2020). Ice extent in sub-arctic fjords and coastal areas from 2001 to 2019 analyzed from MODIS imagery. *Annals of Glaciology*. https://doi.org/10.1017/aog.2020.34

Oggier, M., Eicken, H., Petrich, C., Wilkinson, J., & O'Sadnick, M. (2019). Crude oil migration in sea-ice: Laboratory studies of constraints on oil mobilization and seasonal evolution. *Cold Regions Science and Technology*, 102924.

Petrich, C., & Eicken, H. (2010). Growth, Structure, and Properties of Sea Ice. In D. Thomas & G. Dieckmann (Eds.), *Sea Ice* (2nd ed., pp. 23–78). Oxford: Wiley Blackwell.

Petrich, C., Karlsson, J., & Eicken, H. (2013). Porosity of growing sea ice and potential for oil entrainment. *Cold Regions Science and Technology*, *87*, 27–32.

Petrich, C., Langhorne, P., & Eicken, H. (2011). Modelled Bulk Salinity of Growing First-Year. *Proceedings of the 21st International Conference on Port and Ocean Engineering under Arctic Conditions*.

Petrich, C., O'Sadnick, M. E., & Dale, L. (2017). Recent ice conditions in North-Norwegian porsangerfjorden. *Proceedings of the International Conference on Port and Ocean*

Engineering under Arctic Conditions, POAC.

Porter, S. C. (1989). Some geological implications of average Quaternary glacial conditions. *Quaternary Research*, *32*, 245–261. https://doi.org/10.1016/0033-5894(89)90092-6

Skardhamar, J., Albretsen, J., Sandvik, A. D., Lien, V. S., Myksvoll, M. S., Johnsen, I. A., … Bjørn, P. A. (2018). Modelled salmon lice dispersion and infestation patterns in a sub-arctic fjord. *ICES Journal of Marine Science*, *75*(5), 1733–1747. https://doi.org/10.1093/icesjms/fsy035

Vermote, E. (2015). MOD09A1 MODIS/terra surface reflectance 8-day L3 global 500m SIN grid V006. *NASA EOSDIS Land Processes DAAC*, *10*.

Figures and Tables

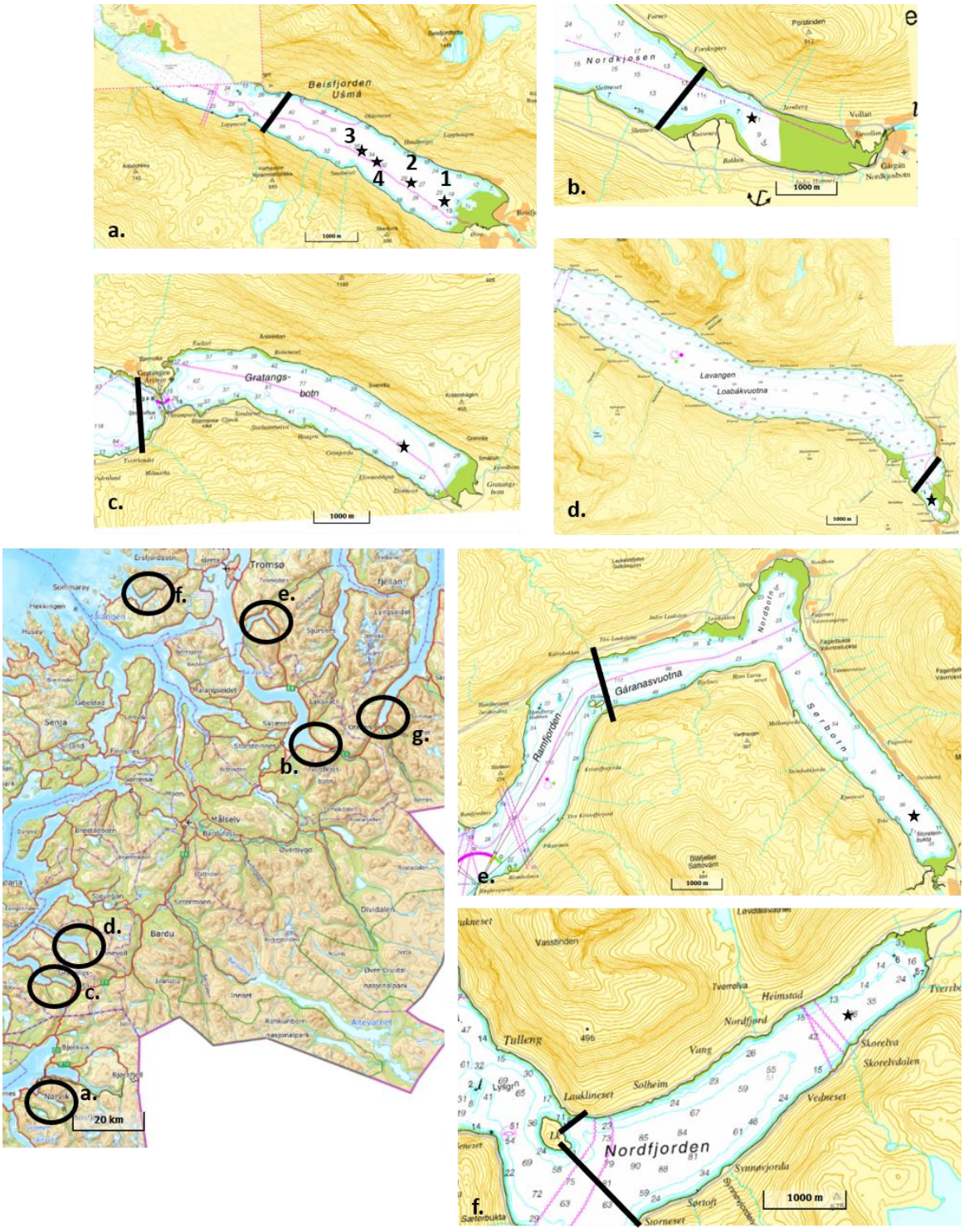

Figure 1. Location of fjords where ice samples were collected, marked with star, with a seventh fjord marked where no ice was present on the day of visit. a) Beisfjord, four locations, marked according to how they are referred in following; b) Nordkjosbotn; c) Gratangsbotn; d) Lavangen; e) Sørbotn/Ramfjord; f) Kattfjord; g) Storfjord (ice- free, no close-up presented).

Figure 2. Example of timelapse images gathered on 6 March 2019 at Beisfjord (top, left), Sørbotn/Ramfjord (top, right), Kattfjord (bottom).

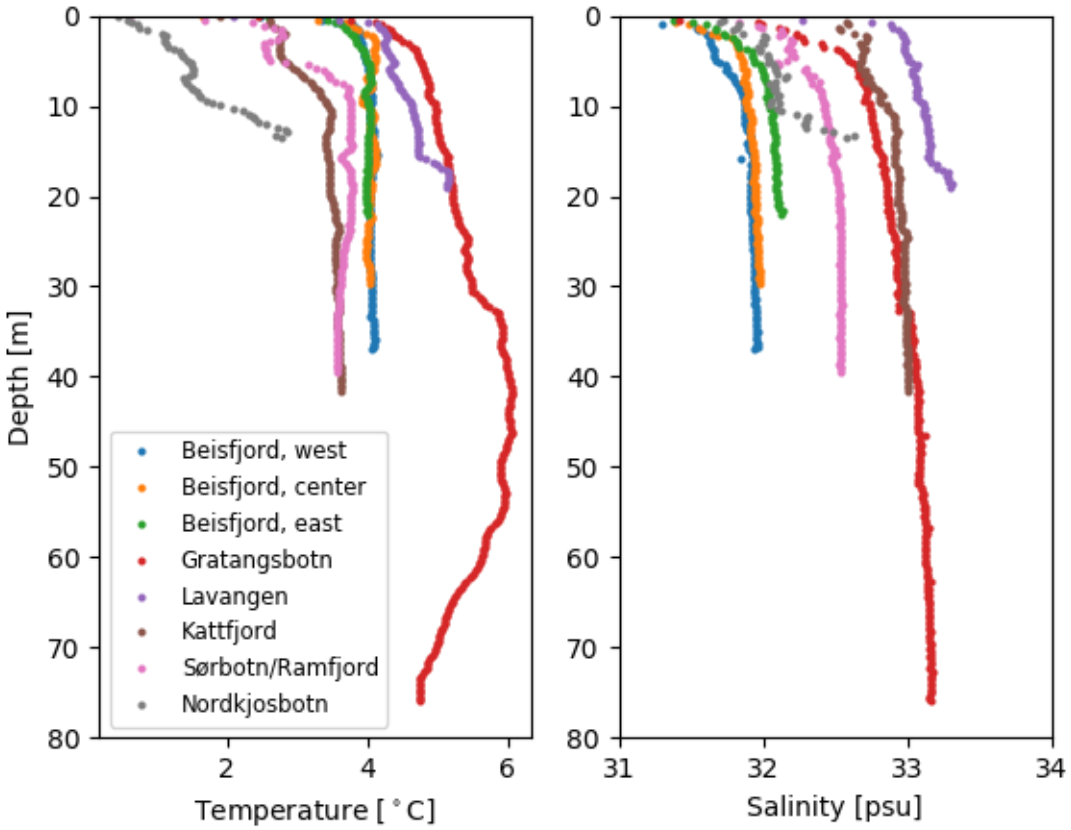

Figure 3. Seawater temperature and salinity under the ice of each core

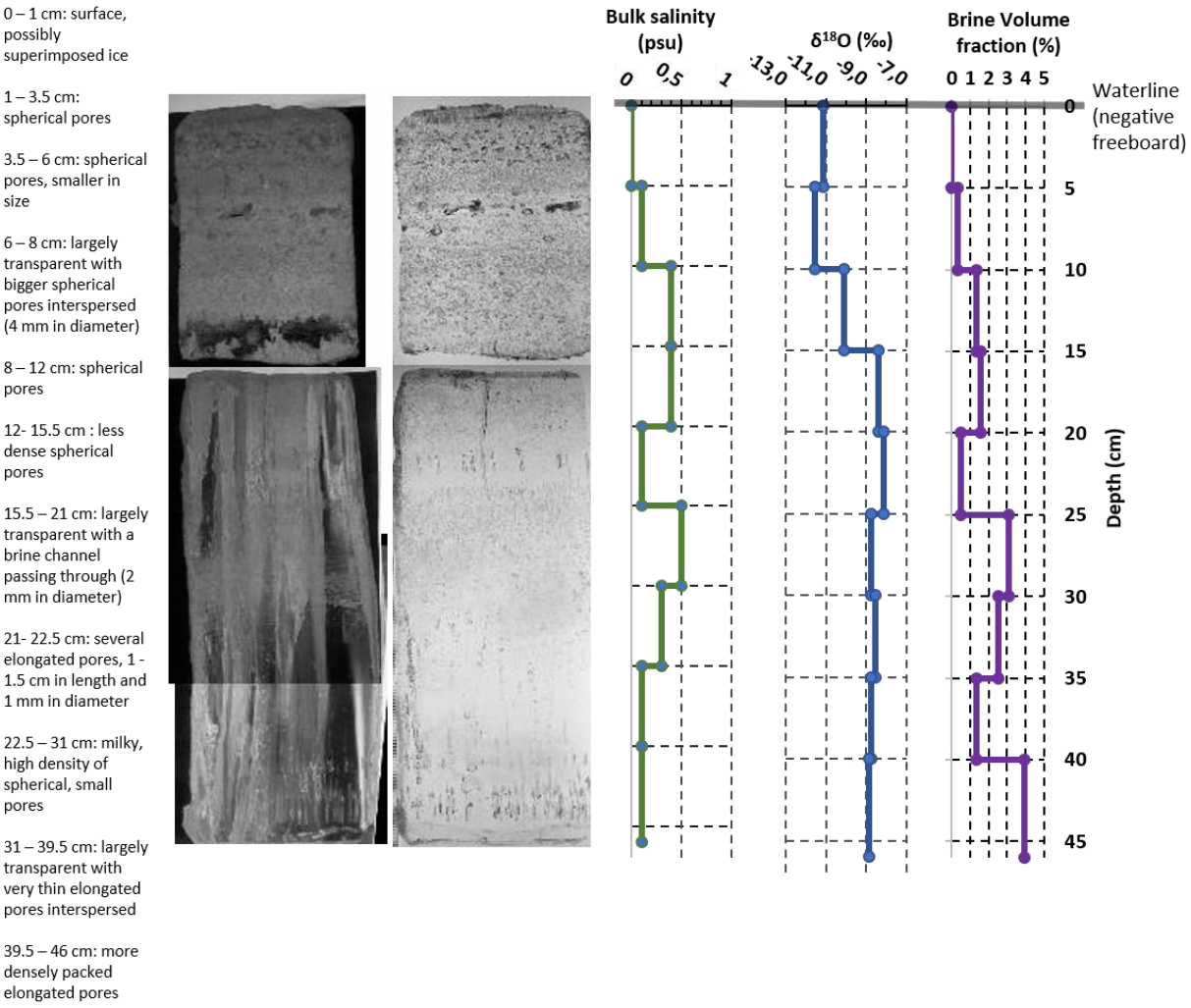

Figure 4. Core sample from Sørbotn/Ramfjord: From left to right- description of layers, cross-polarized imaged, light transmission image, bulk salinity, $\delta^{18}O$, and brine volume fraction.

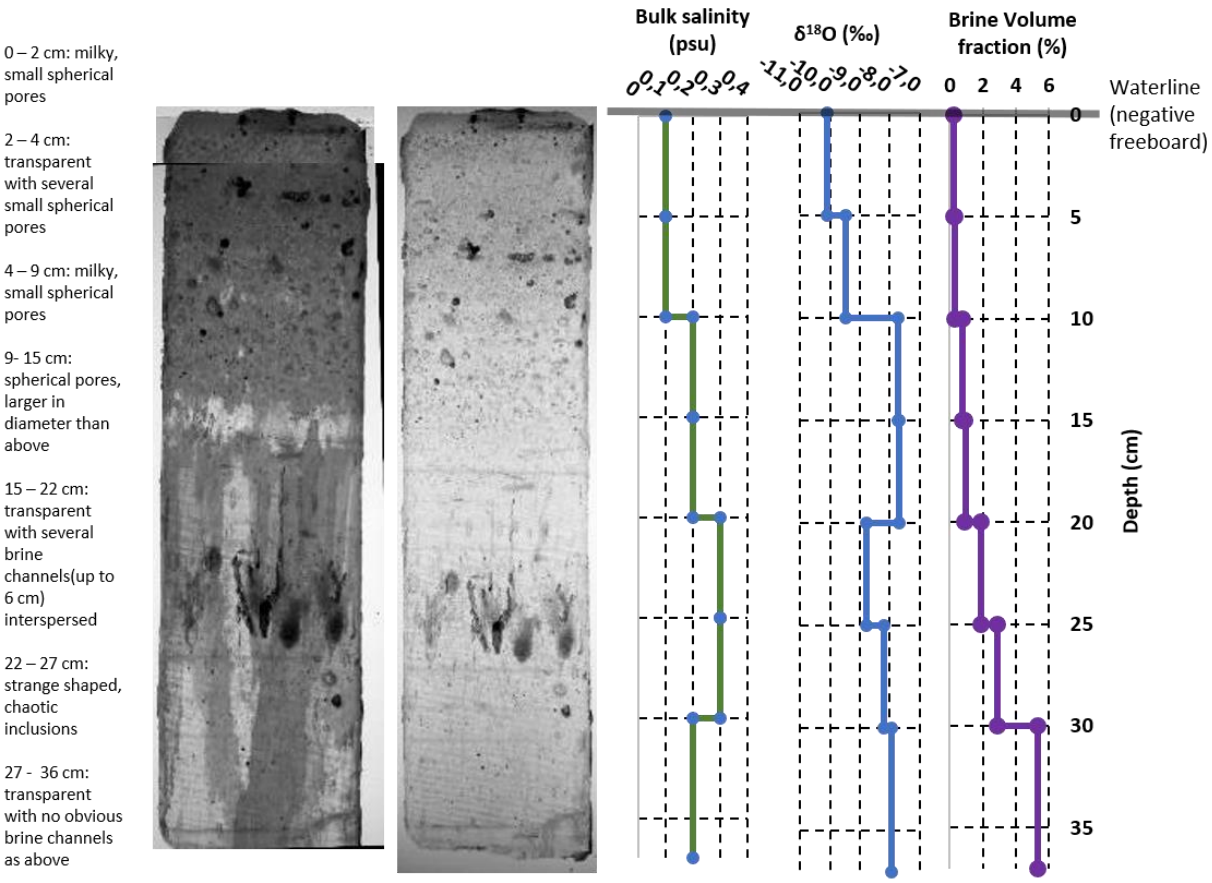

Figure 5. Core sample from Kattfjord: From left to right- description of layers, cross-polarized imaged, light transmission image, bulk salinity, $\delta^{18}O$, and brine volume fraction.

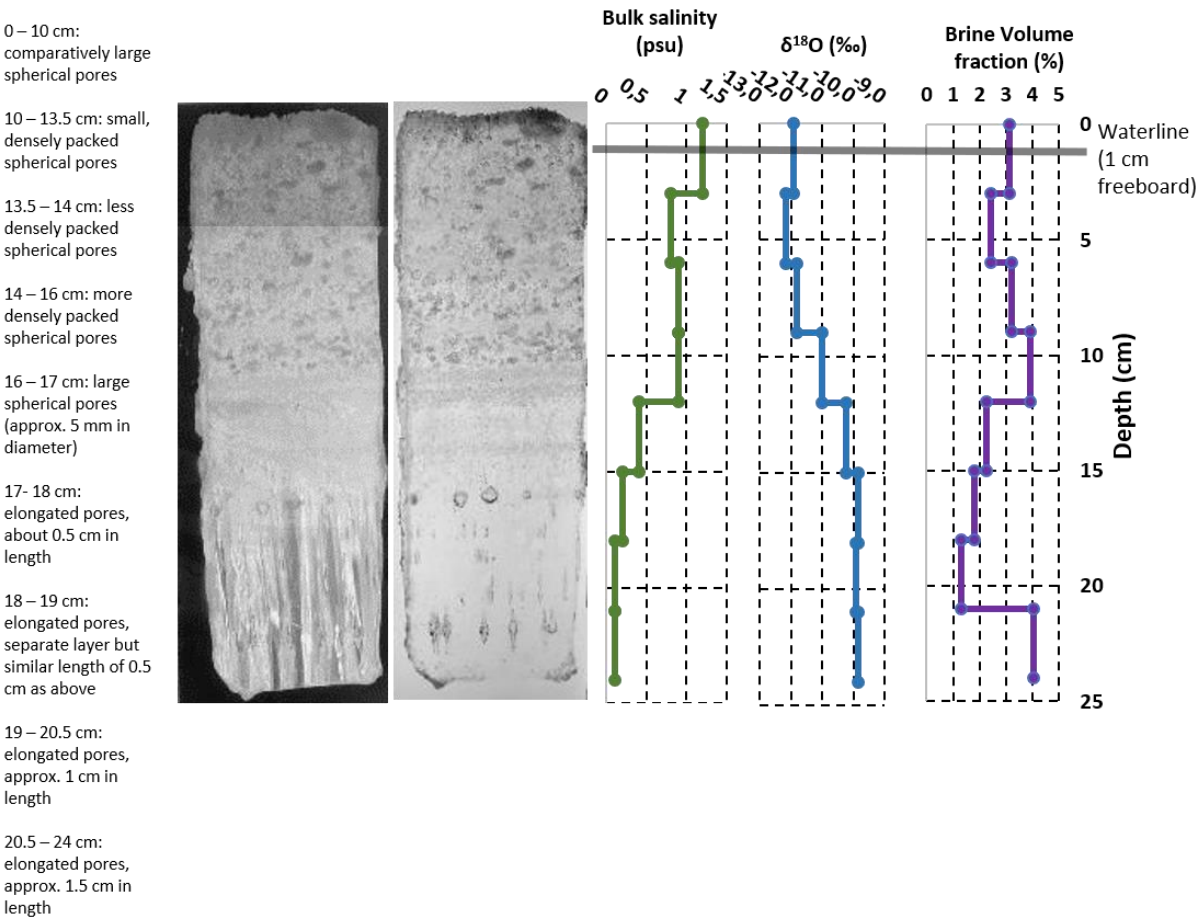

Figure 6. Core sample from Beisfjord 1: From left to right- description of layers, cross-polarized imaged, light transmission image, bulk salinity, $\delta^{18}O$, and brine volume fraction.

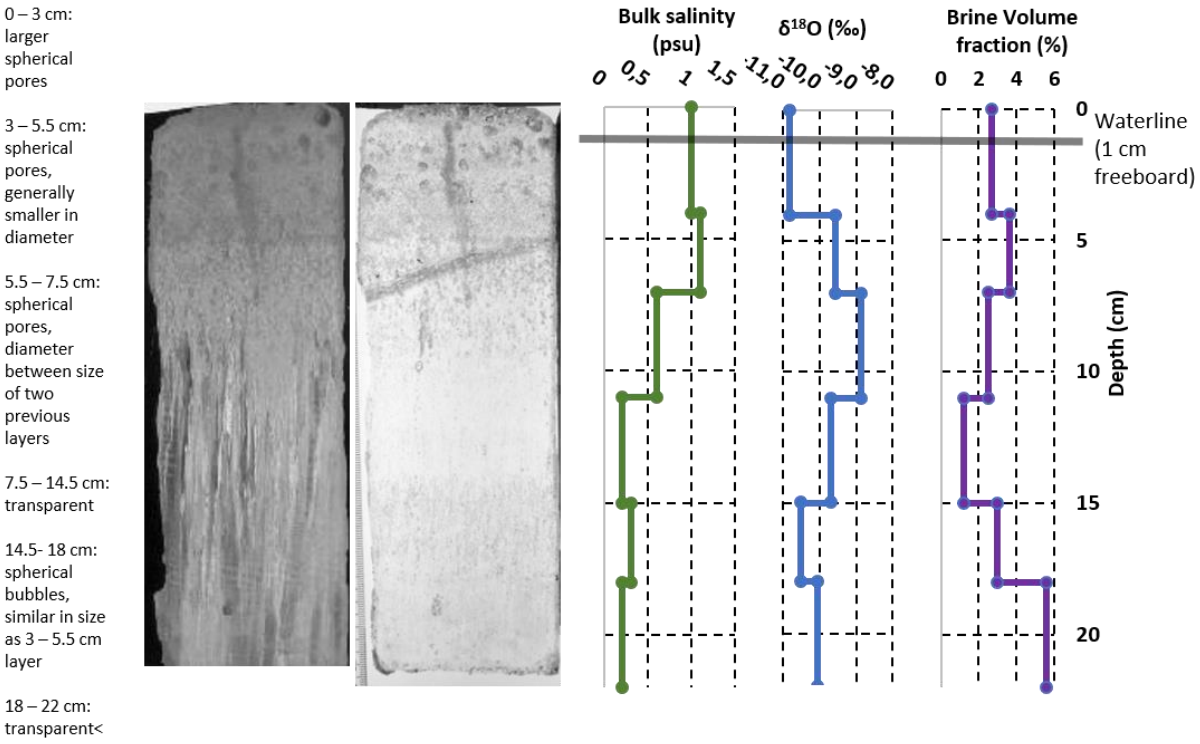

Figure 7. Core sample from Beisfjord 2: From left to right- description of layers, cross-polarized imaged, light transmission image, bulk salinity, $\delta^{18}O$, and brine volume fraction.

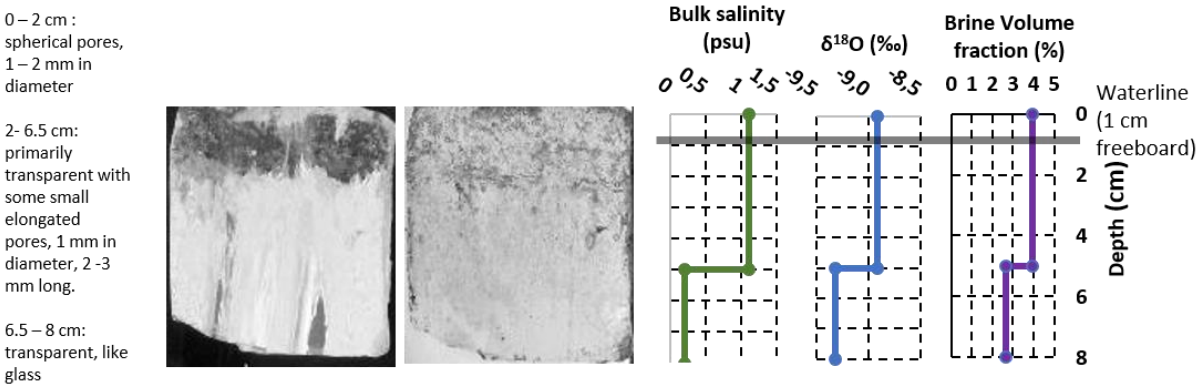

Figure 8. Core sample from Beisfjord 3: From left to right- description of layers, cross-polarized imaged, light transmission image, bulk salinity, $\delta^{18}O$, and brine volume fraction.

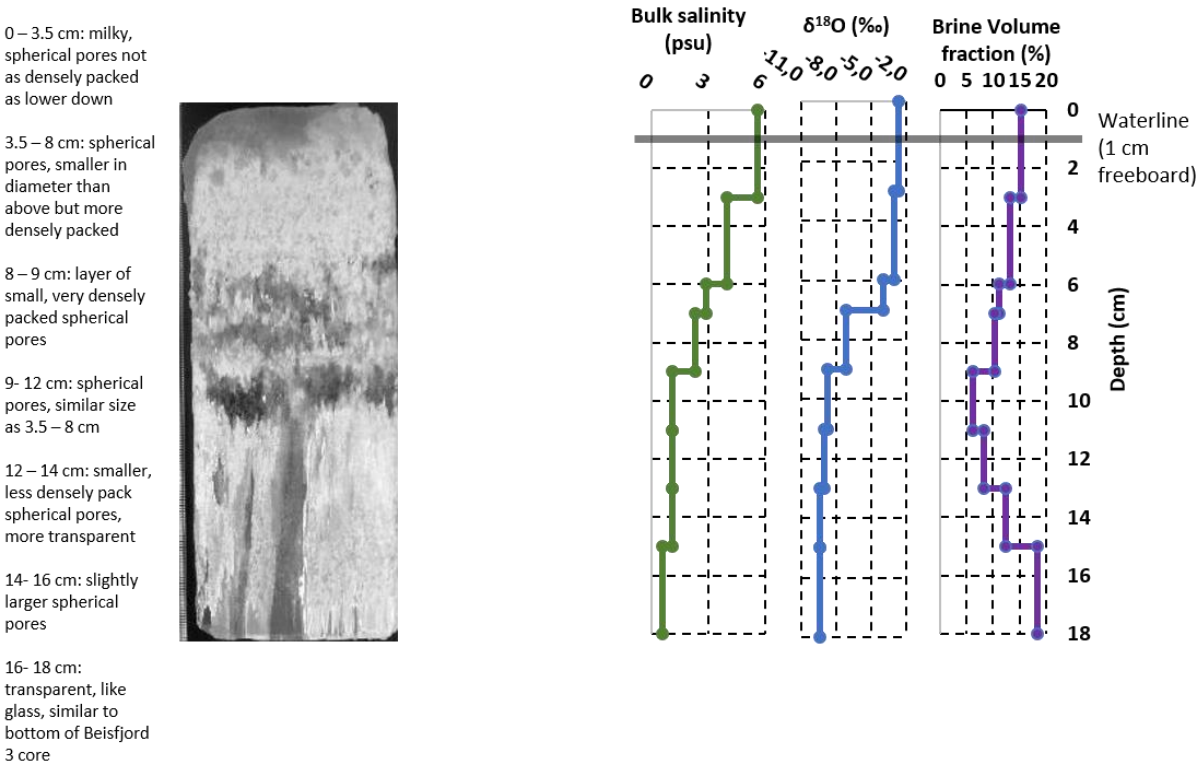

Figure 9. Core sample from Beisfjord 4: From left to right- description of layers, cross-polarized imaged, light transmission image, bulk salinity, $\delta^{18}O$, and brine volume fraction.

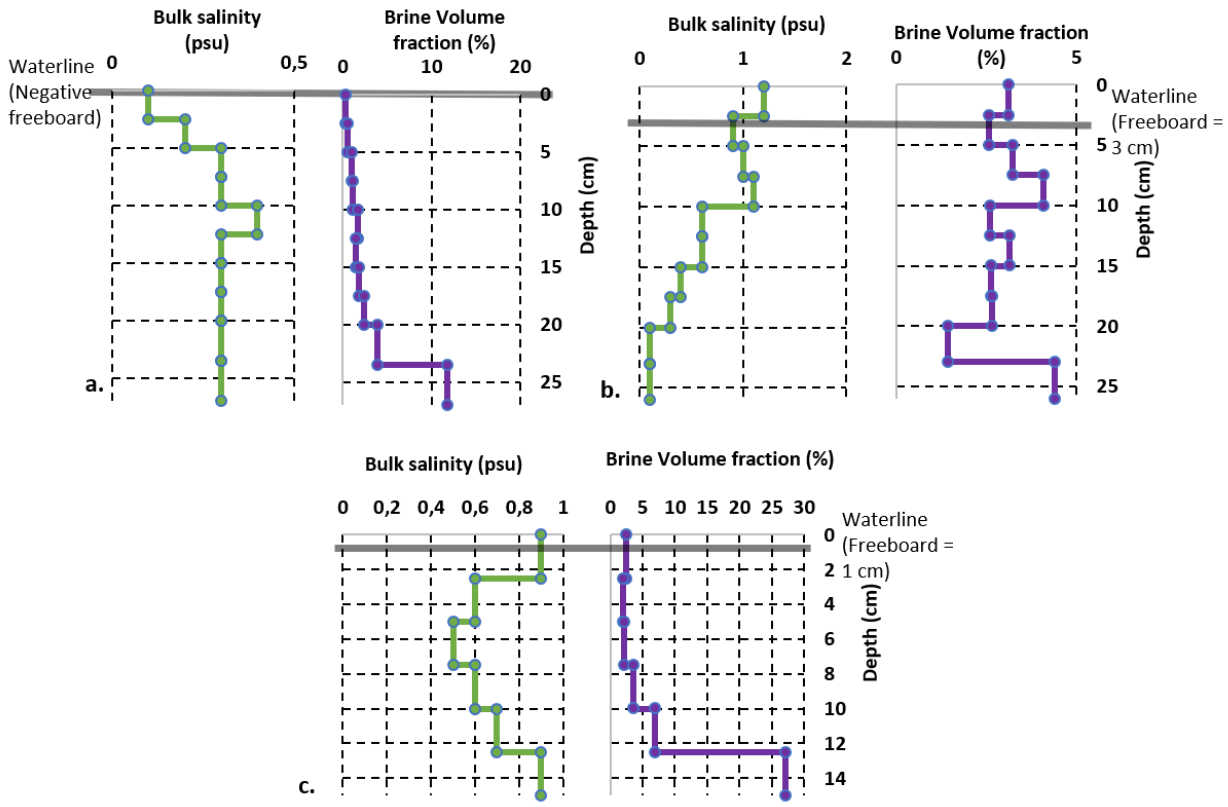

Figure 10. Bulk salinity and brine volume fraction for core samples from a) Gratangsbotn; b) Lavangen; c) Nordkjosbotn

Table 1. Measured ice thickness, freeze-up date, and first day without ice.

Fjord	Ice thickness (cm)	Freeze-Up	Ice Free
Beisfjord	24 (1), 22 (2), 8 (3), 18 (4)	3 March 2019* (from camera)	21 April 2019 (from camera)
Sørbotn/Ramfjord	46	20 December 2018 (from camera)	7 May 2019 (from camera)
Kattfjord	35	14 January 2019 (from camera)	26-27 April 2019 (from camera)
Nordkjosbotn	15	29 – 30 January 2019 (from SAR)	16 – 24 April 2019 (from MODIS)
Lavangen	26	20 – 23 January 2019 (from SAR)	16 – 24 April 2019 (from MODIS)
Gratangen	27	27 – 29 January 2019 (from SAR)	16 - 24 April 2019 (from MODIS)

*Dispersed in bands across fjord, was evidence of ice formation prior near to mouth of fjord but disappeared quickly.

Table 2. $\delta^{18}O$ measurements in ‰ for rivers leading into each fjord and ocean water where ice sampled. Measurement obtained for one ice free fjord, Storfjord, also.

Fjord	River	Ocean
Beisfjord	-12.49	-0.99 (1.0 m)
Sørbotn/Ramfjord	-11.14	-1.06 (0.8 m)
Kattfjord	-10.24	-0.72 (0.8 m)
Gratangen	-10.86	-0.92 (1.0 m)
Nordkjosbotn	-12.15	-0.56 (1.4 m)
Lavangen	-11.34	-0.53 (1.0 m)
Storfjord	-11.55	-0.08 (1.5 m)